CSIRO PUBLISHING

Australian Journal of Physics

Volume 53, 2000

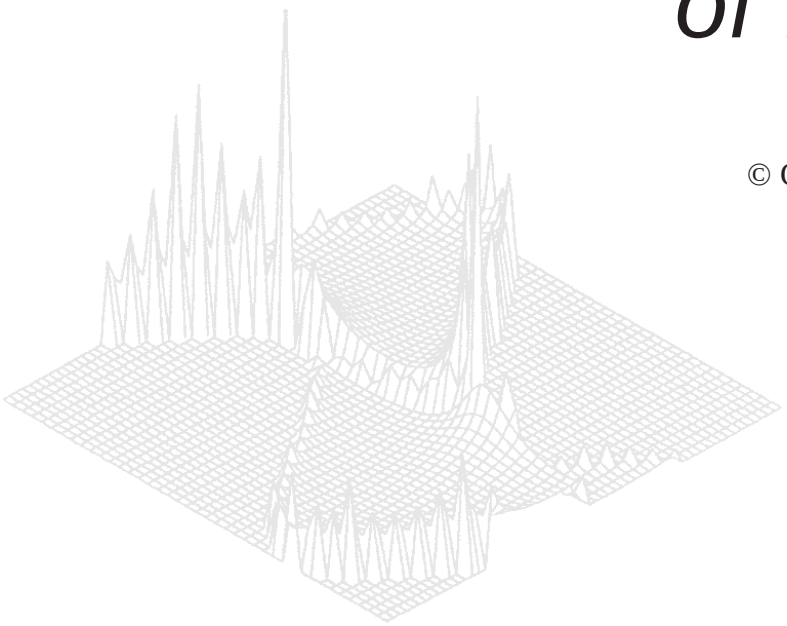

A journal for the publication of
original research in all branches of physics

www.publish.csiro.au/journals/ajp

All enquiries and manuscripts should be directed to
Australian Journal of Physics
CSIRO PUBLISHING
PO Box 1139 (150 Oxford St)
Collingwood Telephone: 61 3 9662 7626
Vic. 3066 Facsimile: 61 3 9662 7611
Australia Email: peter.robertson@publish.csiro.au

Published by **CSIRO** PUBLISHING
for CSIRO Australia and
the Australian Academy of Science

Aust. J. Phys., 2000, **53**, 299–316

Bonding without Ionisation

*E. N. Maslen** *and B. E. Etschmann*

Crystallography Centre, University of Western Australia,
Nedlands, WA 6907, Australia.

Abstract

Charges are calculated for diatomic molecules by partitioning the promolecular density with projection operators derived from free atom potentials. The promolecular charges thus obtained have physically reasonable magnitudes, which are moderately sensitive to interatomic distances and thus to bond type. Their signs are negative for cations and positive for anions. Trends in these charges correlate with subshell structure. Due to the long range of their electrostatic potentials, the cations compete successfully for electrons at the expense of the anions in the density partitioning. This implies that the cation states become overfilled when the atoms overlap, favouring a flow of electrons away from the cation towards the vacant anion states. That accounts for the positive cations and negative anions observed when molecular densities are partitioned with projection operators based on free atom electron densities.

1. Introduction

The well-established role of electron spin pairing, and the close relationship between bond formation and electrolysis (e.g. Partington 1939, 1964; Moore 1939), favours models for bonding based on integral numbers of electrons. The credibility of integral charge models was enhanced when binding energies for alkali halides were predicted semi-quantitatively from the electrostatic (Madelung) energies of arrays of point charges equal in magnitude to the electron's charge (Kittel 1986). Such models representing positively charged cations and negatively charged anions could be fine-tuned by optimising short range repulsive potentials that prevent collapse of the polar point charge lattice. The repulsive terms increase rapidly as the lattice spacing decreases below its equilibrium value.

The binding energy predictions are systematically too large for point charge arrays with signed values derived from cation valencies that exceed unity (Tosi 1964; Trefry *et al.* 1987). Invoking free ions with formal charges in bonding models involves other difficulties that also increase rapidly with atom valence (Zachariasen 1931). Ionisation energies for multiply charged cations are so large that they cannot reasonably be invoked as intermediates in chemical bond formation. Electron affinities for negatively charged monovalent anionic species largely offset ionisation energies required to form positively charged monovalent cations, but the electron affinity changes sign for multiply charged anions (Sherman 1932).

* Deceased.

 10.1071/PH99027 0004-9506/00/020299$10.00

Electron–electron repulsions outweigh the nuclear–electron attractions when the number of electrons on a negatively charged atom exceeds the nuclear charge by two or more.

A strong objection to postulating free ion intermediates in bond formation is that it requires the transfer of bound electrons between atoms, raising the energies for some component entities, whereas the total energy must decrease. A larger energy reduction by interaction between the ionised components must outweigh the net energy gain by all components. Such energy lowering must be related functionally to the energy gains. Unless any large energy gain is functionally linked to reductions, the Boltzmann probabilities for the processes that require that energy gain would be too low.

The extent of charge neutralisation for overlapping ions and its variation with lattice spacing are not defined by the Electroneutrality Principle. In a simple position space superposition of free ion densities, charge cancellation is largely complete (Trefry *et al.* 1987; Buttner and Maslen 1988). It is difficult to differentiate partly cancelling integral charges from charges that are inherently non-integral. Effective charges in solids determined experimentally depend strongly on the measurement technique and its interpretation (Harrison 1980). Those evaluated theoretically depend on the assumptions made. It can be readily understood that physical phenomena depend to differing degrees on the extent and nature of the overlap of charge distributions, but the wide range of values determined for effective charges in the same compound impedes our understanding of charge transfer in chemical bonding.

2. The Promolecule

The term, promolecule, was first introduced by Hirshfeld and Rzotkiewicz (1974). The idea itself, however, was not new, having been used in the calculation of binding energies by Wedepohl (1967) and by Gordon and Kim (1972). The promolecule $\Psi_{\rm pro}$ consists of a product of the free atom wavefunctions ψ_i,

$$\Psi_{\rm pro} = \Pi_i A_i \psi_i \,, \tag{1}$$

where A_i indicates that the ψ_i are antisymmetrised internally. The promolecular concept neglects inter-atom electron quantum-mechanical exchange, and the effect of inter-atom potential terms on the state function, but this approach has nevertheless assisted the understanding of chemical bonding (Hirshfeld 1977*a*). The promolecule's electron density $\rho_{\rm pro}$ is a quasi-quantum-mechanical entity, consisting of superimposed spherically averaged neutral atomic densities ρ_i, with nuclei at the correct coordinates for the molecular system

$$\rho_{\rm pro} = \sum_i \rho_i \,. \tag{2}$$

This provides a useful reference state which allows many chemical and physical properties to be predicted reliably: X-ray and electron scattering powers of gaseous molecules are typical examples. Many global molecular properties can indeed be decomposed into atomic contributions (Balint-Kurti and Karplus 1974; Maksic 1984).

The power of the promolecular model can be partly attributed to the chemical and physical properties that are unique functionals of the one-electron density (Hohenberg and Kohn 1964). The promolecule electron density is much larger than the deformation of the electron density by bond formation. If there exists a relationship between the deformation and total densities, and if that relationship is preserved in an application to a physical property, it should be possible to understand that property qualitatively from a study of the promolecule density alone (Spackman and Maslen 1986).

The promolecule gives a good first order prediction of binding energies for atoms extending across the whole periodic table (Spackman and Maslen 1986). The energies predicted for diatomic molecules containing a monovalent anion and cation at the equilbrium spacing approximate binding energies more accurately than integral point charges at those locations. In so far as promolecule-type energies for diatomic molecules become positive at small interatomic separations, where the nuclear repulsions dominate, the promolecule model includes repulsive components needed to stabilise molecules. The equilibrium separation predicted is smaller than the experimental value for all diatomic promolecules except that for H_2. That results from the neglect of the electron depleting effect of atomic core electrons which overlap with the electron density of the bonded neighbours. The arbitrary nature of the repulsive potential terms added to ionic models to stabilise the system enables them to predict bond lengths more reliably than the promolecule model, but does not necessarily provide improved understanding.

3. Promolecular Charge

The promolecule, being a good first order predictor for a wide range of physical properties, should provide useful preliminary information on charge transfer. While the concept of the promolecule consisting of overlapping free atoms does not define transfer of charge explicitly, the electron density from one atom overlaps with that of other atoms. Geometric partitioning of the electron density, into either discrete or overlapping regions, will not necessarily yield zero charge transfer for the promolecule. The partitioning proposed originally by Hirshfeld generated zero charges for the promolecule by its definition (Spackman and Maslen 1986). To determine the expected charge 'transfer', that is, charge is not physically transferred, it exists only in terms of subdivision of the overlapping electron density, a physical basis for subdividing superimposed electron density between overlapping atoms must be established.

The potential energy components of binding energies $\langle \Psi | V_{\text{bond}} | \Psi \rangle$, where Ψ is the molecular wavefunction, may be expressed in position space as $\int \rho V_{\text{bond}}\, d\tau$, where ρ is the electron density, since in a position space representation V_{bond} is a sum of electrostatic potentials that commute with Ψ. In the promolecule approximation inter-atom exchange correlation and two-electron terms are neglected. The electron density function involved is the one-electron density, and the operator V_{bond} has the form of a Coulomb potential. The electrostatic energy can thus be evaluated by classical electrostatics. Although the corresponding kinetic energy operator does not commute with the state function Ψ, according to the virial theorem the change in kinetic energy due to bonding is simply minus one half times that for the potential energy. Binding energy can thus be well described by evaluating the action of a classical electrostatic potential on a one-electron density.

Promolecule charges can be evaluated by applying a projection operator $w_A(\mathbf{r})$ constructed from free atom electrostatic potentials to the total electron density,

$$w_A(\mathbf{r}) = \frac{V^A_{\text{atom}}(\mathbf{r})}{V_{\text{pro}}(\mathbf{r})}\,, \tag{3}$$

where $V^A_{\text{atom}}(\mathbf{r})$ is the atomic potential of atom A and

$$V_{\text{pro}}(\mathbf{r}) = \sum_{i=\text{all atoms}} V^i_{\text{atom}}(\mathbf{r})\,.$$

The promolecule electron density at every point is allocated to constituent pseudo-atoms in proportion to the free atom electrostatic potential at that location,

$$\rho^i_{\text{pro},V}(\mathbf{r}) = w_A(\mathbf{r})\rho_A(\mathbf{r}) = \frac{V^A_{\text{atom}}(\mathbf{r})}{V_{\text{pro}}(\mathbf{r})}\rho_{\text{pro}}(\mathbf{r})\,. \tag{4}$$

The subdivision is similar to that proposed by Hirshfeld (1977*b*) (equation 6), but the charge is redefined to reflect the contributions of the electron density to the change in potential energy when the atoms overlap to form a molecule. Such operators preserve the total electron density and potential at every point. It would be possible to construct more sophisticated variants, such as 'atomic' potentials modified by electron density lost or accrued, but the simple atomic potential operators provide a first-order picture of charge transfer suitable for the study of molecular systems and simple crystalline solids.

In principle, calculation of promolecular charges ΔQ_{pro} simply involves subtracting the integral of the partitioned electron densities ρ^i_{pro} from the nuclear charge Z_i, yielding

$$\Delta Q_{\text{pro}}(i) = Z_i - \int \rho^i_{\text{pro}}(\mathbf{r})\, d\tau\,. \tag{5}$$

In practice, accurate integration is not necessarily straightforward, as both the potential, and to a lesser extent the electron density, peak sharply at the nuclei.

If the promolecular density were partitioned by an operator proportional to the free atom density,

$$\rho^i_{\text{pro},\rho}(\mathbf{r}) = \frac{\rho_i(\mathbf{r})}{\rho_{\text{pro}}(\mathbf{r})}\rho_{\text{pro}}(\mathbf{r}) = \rho_i(\mathbf{r})\,, \tag{6}$$

the ideal electron count would equal the atomic number, $\int \rho^i_{\text{pro},\rho}(\mathbf{r})\, d\tau = Z$. In practical evaluation the integrated charge may not be the exact number expected (see Table 1). The densities used in these and all other calculations were taken from those tabulated by Mann (1988) and Mann and Waber (1973). Significant errors occur when the rapidly changing electron density functions are integrated numerically. Decreasing the grid size improved the accuracy of the charges, however, the convergence was slow. Thus, a more efficient method of coping with rapidly varying potentials and densities was required.

Table 1. Integrals of partitioned densities (with respect to potential and density) and promolecular charges calculated for NaCl (after correction) at different grid sizes

	Grid size (Bohr)	$\int \rho^i_{\mathrm{pro},V}\, d\tau$	$\int \rho^i_{\mathrm{pro},\rho}\, d\tau$	$\Delta Q_{\mathrm{pro}}(\mathrm{X})$
Na	0·5×0·5	9·769	9·133	11·636
Na	0·25×0·25	11·015	10·399	11·616
Na	0·125×0·125	11·497	10·890	11·607
Cl	0·5×0·5	9·116	9·752	16·364
Cl	0·25×0·25	15·733	16·349	16·384
Cl	0·125×0·125	16·171	16·778	16·393

The error induced by $\int_v \rho^i_{\mathrm{pro},\rho}(\mathbf{r})\, d\tau$ closely approximates that for $\int_v \rho^i_{\mathrm{pro},V}(\mathbf{r})\, d\tau$. The similarity enables the correction for the finite grid size near the nucleus to be evaluated, namely, the error in the integration is

$$\left(\int_v \rho^i_{\mathrm{pro},V}(\mathbf{r})\, d\tau - \int_v \rho^i_{\mathrm{pro},\rho}(\mathbf{r})\, d\tau \right) \times \text{Pixel Volume}\,. \tag{7}$$

Subtracting this error from Z in the equation for $\Delta Q_{\mathrm{pro}}(i)$ above, yields physically reasonable and relatively grid independent promolecule charges (Table 1).

The integration for diatomic molecules proceeded by, first, setting up a grid in cylindrical coordinates, and interpolating the density and potential curves at each point. Cylindrical coordinates were used to utilise the symmetry of the diatomic molecules, where the third coordinate, the angle, could be integrated out. The density and potential at each point were then partitioned, summed, and corrected by the technique described above. The $0{\cdot}5 \times 0{\cdot}5$ bohr^2 grid size sufficed. Evaluating the integrals for these molecules at finer grid sizes was feasible, though more time-consuming. However, evaluating similar charges for crystalline solids using finer grids, being of the order of hours, was inconvenient. When comparing promolecular charges from diatomics and solids at a later stage, it will clearly be preferable to evaluate both by a similar procedure. The coarser $0{\cdot}5 \times 0{\cdot}5$ bohr^2 grid with corrections determined above was therefore preferred. Most interatomic distances were from a compilation of constants for diatomic molecules (Huber and Herzberg 1979), supplemented by Spackman and Maslen (1986).

4. Promolecular Charges for XH and XCl

The promolecular charge $\Delta Q_{\mathrm{pro}}(\mathrm{X})$ for the molecule XY is defined as the charge transferred from atom Y to atom X in partitioning the promolecule electron density with the atomic potential operator (equation 4). Negative $\Delta Q_{\mathrm{pro}}(\mathrm{X})$ thus indicates transfer of electrons from Y to X.

Promolecular charges and experimentally measured bond lengths d_{exp} for the diatomic hydrides, XH, are given in Table 2. The $\Delta Q_{\mathrm{pro}}(\mathrm{X})$ for XH change sign from negative to positive, while the bond lengths decrease monotonically, across each row of the periodic table. The changes in $\Delta Q_{\mathrm{pro}}(\mathrm{X})$ are also monotonic for the first two rows, but not for the third, where $|\Delta Q_{\mathrm{pro}}(\mathrm{Ca})|$ is greater than $|\Delta Q_{\mathrm{pro}}(\mathrm{K})|$. Comparison of the first three periodic table rows reveals that $\Delta Q_{\mathrm{pro}}(\mathrm{X})$ increases with atomic number Z most rapidly for the first row.

Table 2. Diatomic distances and promolecular charges for X in XH

Atom	d (Å)	$\Delta Q_{\mathbf{pro}}$(X)
H	0·74144	−0·000
Li	1·5957	−0·320
Be	1·3426	−0·221
B	1·2324	−0·097
C	1·119	−0·053
N	1·03621	−0·207
O	0·96966	−0·318
F	0·916808	−0·441
Na	1·8874	−0·275
Mg	1·7297	−0·235
Al	1·6478	−0·228
Si	1·52010	−0·150
P	1·42234	−0·049
S	1·3409	−0·026
Cl	1·274552	−0·116
K	2·2425	−0·297
Ca	2·0025	−0·315
Ga	1·6630	−0·186
Ge	1·5880	−0·132
As	1·5344	−0·059
Se	1·475	−0·009
Br	1·414435	−0·057

The $\Delta Q_{\rm pro}$(X) values for chlorides depicted in Table 3 follow trends similar to those for the hydrides in Table 2. Here $\Delta Q_{\rm pro}$(XH) and $\Delta Q_{\rm pro}$(XCl) values correspond to within a scale factor for all three rows of the periodic table, with the exceptions being $-\Delta Q_{\rm pro}({\rm AlCl}) > -\Delta Q_{\rm pro}({\rm MgCl})$, while $-\Delta Q_{\rm pro}({\rm AlH}) < -\Delta Q_{\rm pro}({\rm MgH})$, and the $\Delta Q_{\rm pro}$(CaCl) maximum is global for XCl. This may appear to be insignificant as the error in integration is of the order of 0·03 e- (Table 1), but the Al/Mg effect occurred consistently even when finer grids were used. The $\Delta Q_{\rm pro}$(XCl) increase with Z most rapidly for the first row, as do the $\Delta Q_{\rm pro}$(XH). For the first row $|\Delta Q_{\rm pro}({\rm X})|$ decreases for X = Li, Be, B, whereas in the second row there is a local maximum at Al. On the other hand the bond lengths for the chlorides, after first decreasing as do those for the hydrides, increase slightly at the end of each row.

5. Signs of Promolecule Charges

Although the magnitudes of the $\Delta Q_{\rm pro}$(X) shown in Tables 2 and 3 would be regarded as physically reasonable, it may seem counter-intuitive to those attuned to other pictures of ionic bonding that the $\Delta Q_{\rm pro}$ are negative for cations, and positive for anions. The physical basis for this result is evident from the density and potential curves for Na and F in Fig. 1. Any pair of cations and anions with comparable atomic number show similar trends, as can be seen by examination of the potential profiles (Hall *et al.* 1995).

For small inter-atomic separations R, the electrostatic potential is $V_{\rm F} \sim V_{\rm Na}$, whereas for large R, $V_{\rm F} < V_{\rm Na}$. Bonding is effected when atoms overlap each other, at relatively large R. Due to the cation's extended potential tail it exerts more influence on the overlapping electron density than the anion. The cation

Table 3. Diatomic distances and promolecular charges for X in XCl

Atom	d (Å)	$\Delta Q_{\mathbf{pro}}$(X)
H	1·274552	−0·116
Li	2·020673	−0·756
Be	1·7971	−0·540
B	1·7159	−0·310
C	1·6450	−0·077
N		
O	1·56963	0·225
F	1·628313	0·277
Na	2·360795	−0·616
Mg	2·1991	−0·542
Al	2·130113	−0·552
Si	2·058	−0·382
P		
S		
Cl	1·9879	0·000
K	2·66665	−0·723
Ca	2·4390	−0·786
Ga	2·20169	−0·449
Ge		
As		
Se		
Br	2·136065	−0·063

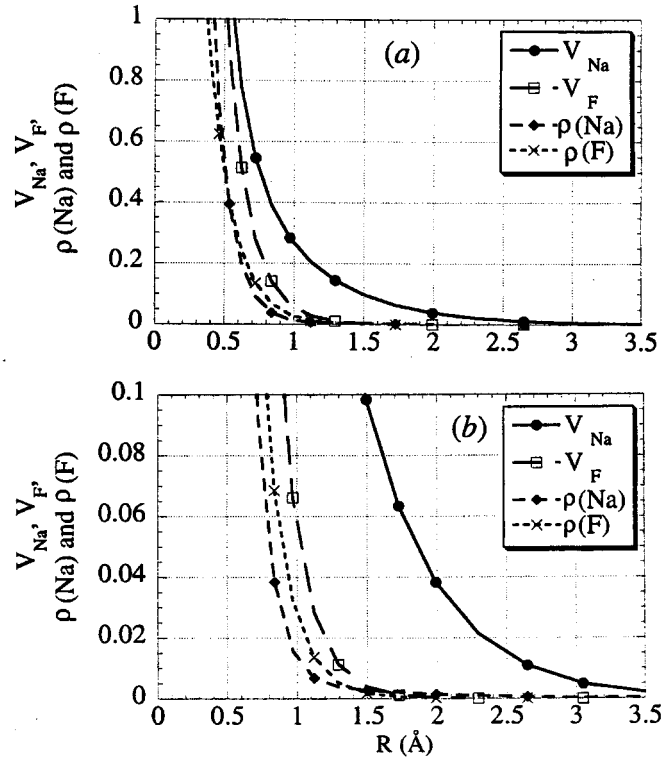

Fig. 1. Curves for (a) the potential (e/Å) and (b) the density (e/Å^3) for Na and F.

competes favourably with the anion for electrons, generating the cation's negative promolecule charge, although no movement of electron density takes place. That is, the negative promolecule charge on the cation and the positive promolecular charge on the anion overlap completely. Charges exist only in terms of subdivision of the overlapping electron density in proportion to the competing potentials.

Most of the accretion of electron density on the cation occurs at large R. In an atomic model that would be viewed as filling holes in the cation's low energy excited states, with mean radii larger than those for its own valence electrons. When atoms condense to form molecules the lower energy excited states of the cation are occupied. Although the total energy is reduced by this condensation, as shown by the calculated promolecule energies (Spackman and Maslen 1986), the energy may be lowered even further by migration of electrons from the occupied excited states of the cations towards the depleted valence states of the anions. That is the basis for the spatial reorganisation of the electron density involved in such physical properties as ferroelectricity, and in the chemical bonding of polar systems. Recognising that the promolecule is a model, prior to bonding, one cause of charge transfer in bond formation is emphasised.

6. Promolecule Charge and Bond Order

Comparison of Tables 2 and 3 shows how the $\Delta Q_{\rm pro}$(X) for X atoms with comparable electronegativity follow similar trends. The effect of bond order (i.e. a single bond versus a double bond) on $\Delta Q_{\rm pro}$(X) may be seen by comparing the $\Delta Q_{\rm pro}$(XF) values in Table 4, with the $\Delta Q_{\rm pro}$(XO), shown in Table 5. It should be noted that not all XO compounds have double bonds, all the group IA and VIIA elements bonded to oxygen are considered to have a single bond.

Table 4. Diatomic distances and promolecular charges for X in XF

Atom	d (Å)	$\Delta Q_{\mathbf{pro}}$(X)
H	0·916808	−0·441
Li	1·563864	−1·023
Be	1·3610	−0·971
B	1·26259	−0·795
C	1·2718	−0·467
N	1·31698	−0·207
O	1·326	−0·094
F	1·41193	0·000
Na	1·925947	−0·782
Mg	1·7500	−0·846
Al	1·654369	−0·945
Si	1·6011	−0·797
P	1·587	−0·579
S	1·600574	−0·427
Cl	1·628313	−0·277
K	2·171457	−0·878
Ca	1·967	−1·069
Ga	1·774369	−0·740
Ge	1·7452	−0·663
As	1·7360	−0·529
Se	1·7408	−0·441
Br	1·75894	−0·330

Table 5. Diatomic distances and promolecular charges for X in XO

Atom	d (Å)	$\Delta Q_{\mathbf{pro}}$(X)
H	0·96966	−0·318
Li	1·728	−0·824
Be	1·3309	−0·918
B	1·2045	−0·751
C	1·128323	−0·471
N	1·15077	−0·161
O	1·20752	0·000
F	1·326	0·094
Na	2·07	−0·658
Mg	1·7490	−0·790
Al	1·6179	−0·909
Si	1·509739	−0·808
P	1·4759	−0·589
S	1·481087	−0·423
Cl	1·56963	−0·225
K	2·22	−0·815
Ca	1·8221	−1·156
Ga	1·7436	−0·701
Ge	1·624648	−0·698
As	1·6236	−0·544
Se	1·6484	−0·430
Br	1·7172	−0·282

There is a strong similarity between both bond lengths and ΔQ_{pro} values for the fluorides and the oxides. All ΔQ_{pro}(X) for XF, except F_2, are negative, increasing monotonically only for the first row, as do those for XH and XCl. Again ΔQ_{pro}(X) increases with Z most rapidly for the first row. The ΔQ_{pro}(XF) and ΔQ_{pro}(XO) are closely similar except that ΔQ_{pro}(OF) is positive. For the first three rows of the periodic table, the ΔQ_{pro}(XO) in Table 5 change non-monotonically with Z. For the second row XF and XO there is a global maximum for $|\Delta Q_{\mathrm{pro}}(\mathrm{X})|$ at Al, and a global maximum at Ca for the third periodic row. The bond lengths for XF and XO have a global maximum at the alkali metals, decreasing to a minimum approximately half way along the row, and then increasing slightly at the end.

The long bond lengths for LiO, NaO and KO are more obvious than those at LiF, NaF and KF respectively. That difference in bond lengths reflects the fact that the O atom forms double bonds with divalent atoms, whereas the F atom is limited to single bonds. The ΔQ_{pro}(LiO), ΔQ_{pro}(NaO) and ΔQ_{pro}(KO) are notably less negative than ΔQ_{pro}(LiF), ΔQ_{pro}(NaF) and ΔQ_{pro}(KF), reflecting the more extended density and potential of the O atom, and the inability of the alkali metals to form double bonds. This effect could be ascribed to more effective electron spin pairing in the alkali halides, or in other words, as illustrating the "stability of the closed sub-shell" for the F atom. Alternatively it can be argued that the F atom's core is smaller and the effective nuclear charge in the valence shell larger than that in the O atom. Bond length reducing effects would be offset by increased exchange repulsions between the overlapping electrons for the anionic fluorides. The second hypothesis accounts for the small but perceptible lengthening of XF, compared with XO, for X on the electronegative side of the periodic table.

Data for the transition metal oxides are compiled in Table 6. The charges are smaller in magnitude than those for the main body XO, which can be attributed to the shielding of the transition metals' $3d$ electrons, and the subsequent reduction in overlap with bonded neighbours.

Table 6. ΔQ_{pro}(T) at experimental bond lengths

Atom	d (Å)	ΔQ_{pro}(T)
Ca	1·8221	−1·156
Sc	1·66826	−1·203
Ti	1·62022	−1·156
V	1·58932	−1·099
Cr	1·615	−0·996
Mn	1·769	−0·788
Fe	1·6395	−0·836
Co		
Ni		
Cu	1·72437	−0·545
Zn		

7. Promolecular Charge and Core Structure

The ΔQ_{pro}(X) versus X slope for the series XA (where A is H, Cl, F or O) appears to depend on the core structure of the X atom involved. The slope for the first row atoms with their simple $1s^2$ core is invariably steeper than that for the higher rows, whereas gradients for the second row are only slightly larger than those for the third. This implies that the core density near the effective atomic radius decreases more rapidly for $1s^2$ cores than for the ns^2np^6 cores. Relative to the core, the first row atoms' valence shells extend further, allowing the cations to 'acquire control' of more valence electrons from their bonded neighbours.

The consistent break in correlation trends for promolecular charges involving alkali metals at Li (e.g. Tables 2 to 5) is also consistent with significant dependence of properties on core structure. This result is not just an artefact in these calculations. Physical and chemical properties of the alkali metal elements, such as electrical and thermal conductivities, also change more rapidly from the first to the second than between second and third, third and fourth rows (Sargent-Welsh Periodic Table 1980), as shown in Table 7.

Table 7. Comparison of physical properties of the alkali metals

		Li	Na	K	Rb	Cs
Electrical cond.	(10^6/Ω cm)	0·108	0·210	0·139	0·0779	0·0489
Thermal cond.	(W/cm K)	0·847	1·41	1·024	0·582	0·359

The ΔQ_{pro} and bond lengths for the transition metal hydrides are listed in Table 8. The H atom is atypical of chemical bonding generally, as it lacks a core, and thus an exclusion zone for other atom's valence electrons. The ΔQ_{pro}(XH) for diatomic hydrides reflect the special chemical and physical properties of hydrogen. The ΔQ_{pro}(XH) for hydrides are small because H, having a single valence electron, can 'lose' no more than one electron, whereas true halogen

atoms, having one hole in their valence sub-shell, can potentially transfer more than one electron and thus have $\Delta Q_{\rm pro}$ larger than unity. However, hydrogen differs far more from the alkali metals than the halogens by having the positive $\Delta Q_{\rm pro}$ typical of anions.

Table 8. $\Delta Q_{\rm pro}$(T) at experimental bond length distance (for TH)

Atom	d (Å)	$\Delta Q_{\rm pro}$(T)
Mn	1·7311	−0·222
Ni	1·4756	−0·182
Cu	1·46263	−0·140
Zn	1·59490	−0·141

8. Promolecule Charge and Subshell Structure

While differences between the first, second and third rows are related to changes in the core structure, systematic variation in the slope of the $\Delta Q_{\rm pro}$(X) versus Z curve within each row can be related to the electron density for the X atoms involved. This is largely an outer-shell effect which can be seen from the second moments of the proatomic densities, defined as

$$\langle r^2\rangle = \frac{1}{N}\int r^2\rho_{\rm pro}(\mathbf{r})\,d\mathbf{V} = \frac{\int r^4\rho_{\rm pro}(\mathbf{r})\,d\mathbf{r}}{\int r^2\rho_{\rm pro}(\mathbf{r})\,d\mathbf{r}}\,, \tag{8}$$

where N is the number of electrons, which are shown in Table 9. The second moment of the atomic density can be related to effects such as diamagnetic susceptibilities, polarisabilities and mean inner potential (Tsirelson and Ozerov 1996). Atomic properties correlate well with $\Delta Q_{\rm pro}$(X), derived from densities for diatomic promolecules, depicted in Tables 2 to 5.

Table 9. Values of $\langle r^2\rangle$ of the proatom electron density

Atom	$\langle r^2\rangle$	Atom	$\langle r^2\rangle$
H	0·840	Si	0·661
Li	1·739	P	0·582
Be	1·212	S	0·513
B	0·887	Cl	0·454
C	0·664	K	0·751
N	0·503	Ca	0·787
O	0·395	Ga	0·364
F	0·318	Ge	0·366
Na	0·690	As	0·353
Mg	0·689	Se	0·337
Al	0·719	Br	0·321

The $\langle r^2\rangle$ decrease monotonically from Li to F, as does $-\Delta Q_{\rm pro}$(X) for the fluorides (Fig. 2), hydrides and chlorides. Along the second row, both $\langle r^2\rangle$ and $-\Delta Q_{\rm pro}$(X) for the fluorides and oxides (with minor variations for XH and XCl) increase from Na to Al, and then decrease to Cl. The increase in $-\Delta Q_{\rm pro}$(X)

that occurs from K to Ca and the subsequent decrease to Br (for XF, XO, XH and XCl) are again consistent with trends in the atomic second moments.

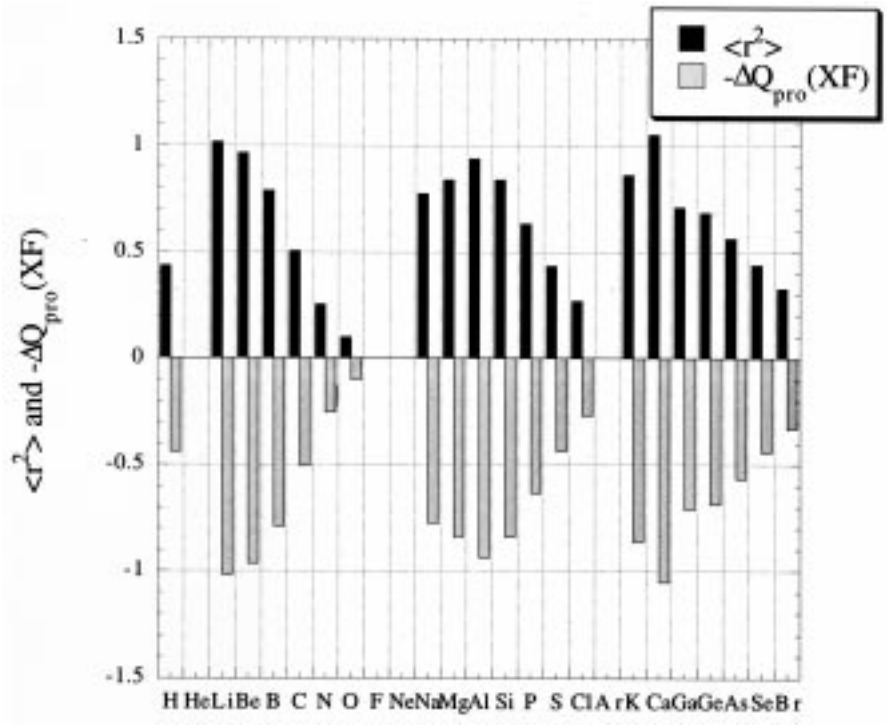

Fig. 2. Values of $\langle r^2 \rangle$ and $-\Delta Q_{\mathrm{pro}}(\mathrm{XF})$.

In accounting for the topographical characteristics of the $\Delta Q_{\mathrm{pro}}(\mathrm{X})$ versus Z curve within each row, consider for example K and Ca. Ca has two valence electrons in the $3s$ subshell, whereas K has only one. Increased electron–electron repulsion causes the Ca subshell to expand, as is reflected in the distribution function of its two s state valence electrons. That generates the increased value of $-\Delta Q_{\mathrm{pro}}(\mathrm{CaH})$, $-\Delta Q_{\mathrm{pro}}(\mathrm{CaCl})$, $-\Delta Q_{\mathrm{pro}}(\mathrm{CaF})$ and $-\Delta Q_{\mathrm{pro}}(\mathrm{CaO})$, shown in Tables 2 to 5 respectively. This effect is reflected in Table 9, where the second moment of Ca is greater than K. The same effect is expected to occur between Na and Mg, however, $\langle r^2 \rangle_{\mathrm{Na}}$ is the same as $\langle r^2 \rangle_{\mathrm{Mg}}$. The value of $-\Delta Q_{\mathrm{pro}}(\mathrm{Na})$ is less than $-\Delta Q_{\mathrm{pro}}(\mathrm{Mg})$ for the fluorides and oxides, but not for the hydrides and chlorides.

For all four series, XF, XO, XH and XCl, we have $-\Delta Q_{\mathrm{pro}}(\mathrm{Al}) > -\Delta Q_{\mathrm{pro}}(\mathrm{Mg})$. Why is $-\Delta Q_{\mathrm{pro}}(\mathrm{Al})$ consistently larger? This is again reflected in the second moments, where Al is larger than Mg. Extending that argument, it can be seen that Si has a smaller $\langle r^2 \rangle$ than Al, thus the promolecular charges $-\Delta Q_{\mathrm{pro}}(\mathrm{Si})$ are smaller in magnitude than $-\Delta Q_{\mathrm{pro}}(\mathrm{Al})$.

The decrease in $-\Delta Q_{\mathrm{pro}}(\mathrm{X})$ from Ca to Ga, compared to the increase from Mg to Al, can presumably be attributed to the intrinsic difference in the subshell structure for the two rows. Al ($3s^2 3p^1$) has only one more electron than Mg ($3s^2$), but Ga ($3d^{10} 4s^2 4p^1$) contains an additional filled $3d$ subshell, compared to

Ca ($4s^2$). The filled $3d$ subshell appears to cause Ga to become more strongly anionic, as can be seen by comparing the potential curves of Al and Ga in Fig. 3. While the curves effectively overlap, the bond lengths of GaX are greater than those of AlX, implying that Ga is more anionic than Al.

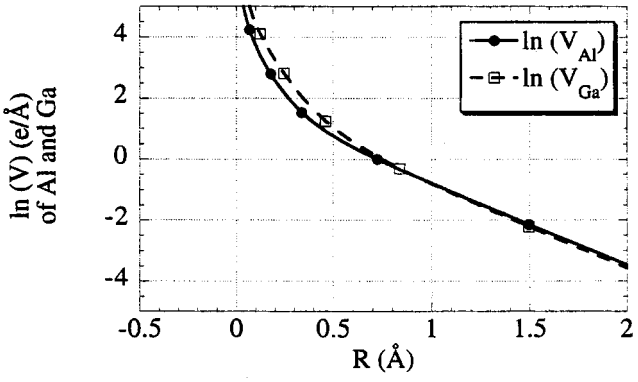

Fig. 3. Potential curves (e/Å) for Al and Ga.

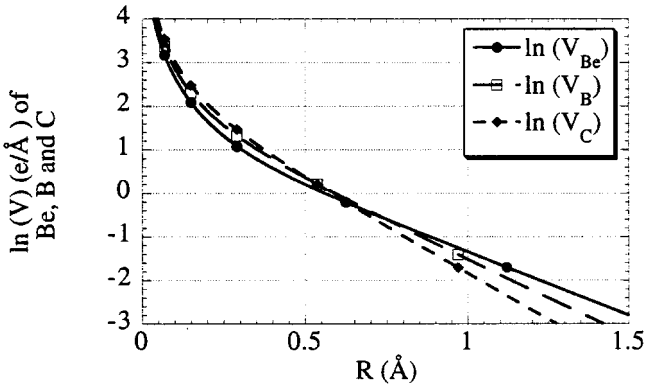

Fig. 4. Potential curves (e/Å) for Be, B and C.

9. Metals versus Non-metals

It is well known that the metallic properties of elements, such as electrical and thermal conductivity, decrease across the rows of the periodic table. To the left of a 'diagonal line' in the table, the elements are metals, those to the right are non-metals, with elements near the boundary generally classified as 'semi-metals'.

The rather abrupt transition from metal to non-metal can be related to differences in electronegativity. An equivalent explanation is provided by the potential curves. Potentials at large R for non-metals are lower than that for the nearest metal. Thus, of the potentials for Be, B and C shown in Fig. 4, V_{Be} is the smallest at low R, but exceeds V_{B} and V_{C} as R increases. At $R \sim 0{\cdot}7$ Å, V_{Be} becomes larger than those for the non-metals. Similarly, examination of the electrostatic potential curves for Mg, Al, Si and Ge, As, Se reveals that the metal has a higher large R potential than the non-metal.

Metals are distinguished from non-metals more definitely by trends among the promolecular charges, as indicated in Table 5. For the first row oxides there are two distinct slopes, a negative slope from Li to Be and a positive slope from B to F. The discontinuity in slope of the $\Delta Q_{\rm pro}(\rm X)$ versus Z curve from one element to the next coincides with a change from metal to non-metal.

For the second row oxides the negative slope from Na to Al and the positive slope from Si to Cl is consistent with this hypothesis. The third row oxides reinforce this trend. There are effectively three slopes: a negative gradient from K to Ca, a flat slope from Ga to Ge, and a positive slope from As to Br. The discontinuity after Ca marks the start of the first transition series. The second occurs at the metal/non-metal boundary.

While the promolecular charge for the first row fluorides (Table 4) decreases monotonically with atomic number, there are two distinct slopes, from Li to Be and from B to F. The second row exhibits the same pattern as the oxides. In the third row there is the standard break after Ca, but the slope from Ga to Br changes smoothly, any discontinuity at the metal/non-metal boundary being less marked. The slopes for the first row oxides and fluorides from B to F are linear from B to N, but tail off from O to F.

In contrast with the oxides and fluorides, the $-\Delta Q_{\rm pro}(\rm X)$ values for the first row hydrides (Table 2) increase linearly from Li to F. The second row shows a discontinuity at Mg/Al consistent with the hypothesis described above, and the third row follows the same trend as the fluorides.

For the first row chlorides the $\Delta Q_{\rm pro}(\rm X)$ versus Z curve (Table 3) has a linear slope from Li to C. In the second row the promolecular charge magnitude decreases from Na to Mg and then increases slightly from Mg to Al, decreasing from Al to Si.

Although slope discontinuities in the $\Delta Q_{\rm pro}(\rm X)$ versus Z curve do not identify metal/non-metal transitions unambiguously in every case, the association is strong. When factors such as electronegativity differences and atomic size are accounted for accurately, the relationship betwen slope discontinuities and metal/non-metal transitions may well become unique.

10. Promolecular Charges and Row Number

Tables 2 to 5 show that $\Delta Q_{\rm pro}(\rm X)$ values for atoms in the same column decrease with Z in many cases, reflecting the expected trend for atoms to be more electropositive as Z increases. The $\Delta Q_{\rm pro}(\rm X)$ values become correspondingly more negative as the electronegativity χ is reduced.

Promolecular charges and bond lengths for the alkali halides, given in Table 10, show variations less typical of the trend with row number. All the $\Delta Q_{\rm pro}(\rm X)$ values for the alkali halides are negative. Careful examination reveals that the variation of the $-\Delta Q_{\rm pro}(\rm X)$ with row number is larger for the fluorides than that for chlorides. There is no simple correlation between $\Delta Q_{\rm pro}(\rm X)$ and bond length for these alkali halides. However, comparison of the $\Delta Q_{\rm pro}(\rm X)$ for alkali metal cations with given halogen anions reveals a consistent trend. The largest $-\Delta Q_{\rm pro}(\rm X)$ occurs at Li. The promolecular charge decreases from Li to Na, and increases slightly to K.

The consistent local maximum at Li and minimum at Na implies a slope of the $\Delta Q_{\rm pro}(\rm X)$ versus Z curves that is positive rather than negative. The origin

of the lesser electron attracting power of Na is not evident from the potential curves, calculated from the densities (Mann 1988; Mann and Waber 1973) shown in Fig. 5, where $V_{\mathrm{Li}}(\mathbf{r})$ is relatively less extensive than $V_{\mathrm{Na}}(\mathbf{r})$ when the radii of the atoms are considered. The low electron attracting power of Na relative to Li must reflect subtle differences originating in the $1s^2$ core structure for Li, and the $1s^2 2s^2 2p^6$ for Na.

Table 10. Promolecular charges and bond lengths for alkali halides

AB	d (Å)	$\Delta Q_{\mathrm{pro}}(\mathrm{A})$
LiF	1·564	−1·023
NaF	1·926	−0·782
KF	2·171	−0·878
LiCl	2·021	−0·756
NaCl	2·361	−0·616
KCl	2·667	−0·723
LiBr	2·170	−0·702
NaBr	2·502	−0·579
KBr	2·821	−0·691

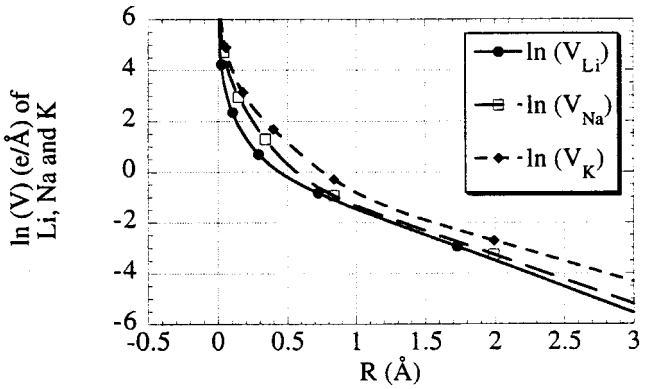

Fig. 5. Potential curves (e/Å) for Li, Na and K.

11. Alkali Diatomics

The small changes in $\Delta Q_{\mathrm{pro}}(\mathrm{X})$ arranged as series down the columns of the periodic table imply that the charges for diatomics involving atoms in the same column of the table should also be small. Table 11 shows that the $\Delta Q_{\mathrm{pro}}(\mathrm{X})$ values for alkali metal diatomics are an order of magnitude smaller than those for the alkali halides, as expected. That is due to the difference in electronegativity between alkali metals being less than that between metals and halogens.

Table 11. Bond lengths and promolecular charges for alkali diatomics

AB	d (Å)	$\Delta Q_{\mathrm{pro}}(\mathrm{A})$
LiNa	2·81	0·008
LiK	3·27	0·054
NaK	3·589	0·057

Although the electron attracting power is a minimum for Na, the results are not wholly as expected from the alkali halides, which indicate that the electron attracting power of Li and K atom are comparable. In the metal diatomics the K atom attracts electrons from Na but also from Li. The small difference in those cases is reflected in the number of electrons attracted by Li from Na. There appears to be a correlation of $\Delta Q_{\mathrm{pro}}(\mathrm{X})$ with bond length among these atoms. The shorter the bond, the less the charge transfer, as shown in Table 11. That result is not consistent with the trends reported above for the more strongly hetero-polar diatomics.

12. Ions versus Neutral Atoms

The ionic model is based on the premise that free atoms gain or lose electrons, and the subsequent ions combine to form molecules or lattice structure. While this model has successfully explained many properties, such as the electrochemical series, it has limitations. The most serious of these is the question of the extent to which free ions actually can exist in chemical combination. Perhaps the greatest difficulty is that multiply charged negative ions such as O^{2-} and N^{3-} are unstable. Repulsion between excess electrons invariably outweighs the energy lowering when those electrons combine with the free atom.

It is possible to use an ionic model as the basis for charge partitioning identical in principle to that based on the promolecule. In order to compare promolecule charges based on the promolecular and ionic models, electron densities were calculated for Li and Li^+, Na and Na^+, F and F^-, and for Cl and Cl^- using the Roothaan–Hartree–Fock (RHF) wavefunctions of Clementi and Roetti (1974). The atomic electron densities differ almost imperceptibly from the values evaluated by Mann (1988; Mann and Waber 1973) who used numerical wavefunctions in the calculations described above.

The potentials for Na^+ and F^- plotted along with the atomic potentials (derived from the Mann radial densities) in Fig. 6, were used to partition the sum of ionic electron densities in a manner identical to that applied for the promolecule constructed from neutral atoms. For the neutral atom case, the projection operators that subdivide the electron density are by definition confined to be between $0{\cdot}0$ and $1{\cdot}0$. Constraints were required to achieve that in the domain where the charged anion potential was negative. The projection operators $V_{\mathrm{Na}^+}/(V_{\mathrm{Na}^+} + V_{\mathrm{F}^-})$ and $V_{\mathrm{F}^-}/(V_{\mathrm{Na}^+} + V_{\mathrm{F}^-})$ subdivide the sum of the electron densities for free Na^+ and F^- ions. Elements of that density, for which the operator $V_{\mathrm{F}^-}/(V_{\mathrm{Na}^+} + V_{\mathrm{F}^-})$ for the anion was negative, were considered to be repelled from the anion, and assigned totally to the cation. That is, the projection operators for the cation and anion were set at $1{\cdot}0$ and $0{\cdot}0$ respectively in such cases. Where the promolecular potential $V_{\mathrm{Na}^+} + V_{\mathrm{F}^-}$ was negative, the density was assigned to the cation which invariably had the greater potential in that domain. As the anion potentials became negative at distances less than the interatomic separation, the convergence of the summations was determined solely by the electron density function.

The signs of the charges calculated from the ionic densities and potentials were the same as those obtained by partitioning neutral atom densities with neutral atom potentials, but their magnitudes were far greater, as can be seen in Table 12. Anion charges have the same magnitude as the cations, but have opposite, i.e. positive, signs.

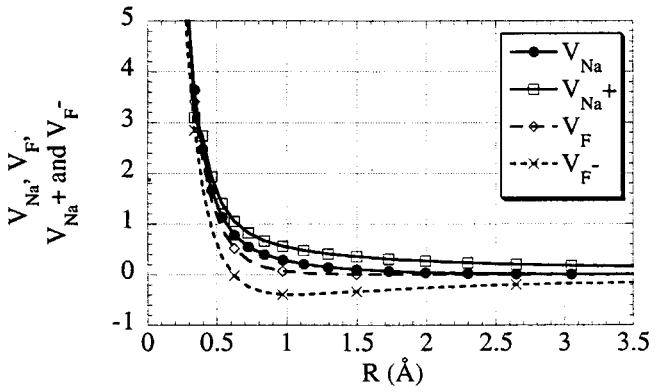

Fig. 6. Potential curves (e/Å) for Na and F: atoms versus ions.

Table 12. Comparison of promolecular charges obtained using neutral and ionic densities

AB	d (Å)	$\Delta Q_{\rm pro}$(A) ionic	$\Delta Q_{\rm pro}$(A) neutral
NaF	1·926	−2·351	−0·782
NaCl	2·361	−7·255	−0·616
LiF	1·564	−3·124	−1·023
LiCl	2·021	−5·712	−0·756

Partitioning the sum of free ion densities based on ionic potentials thus reverses the sign of the charges assumed initially, but yields unphysically large values due to the very short radius for which the negatively charged anion's potential remains positive. The differences in charge when the F anion is replaced by Cl become unphysically large for both Na and Li, in marked contrast to the charges evaluated with neutral atom potentials, where unit changes in the row or column of the periodic table produce changes in promolecule charge of not more than 0·3 electrons. These anomalous charge differences are typical difficulties that may be encountered when charged pseudo-atoms in molecules are modelled by free ions.

13. Conclusions

The promolecule model favours the following mechanism for charge transfer in bonding. Due to the long range electrostatic potential, cations compete so successfully for electrons that the cation states are overfilled. As the low energy excited states for these atoms are occupied, those cations become unstable. The nuclear electrostatic attraction suffices to 'hold' slightly more than Z electrons successfully. Meanwhile the anion valence states are depleted. Electrons flow from the negatively charged, overfilled excited cation states towards the positive, depleted valence anion states. That flow of electrons in position space is distinct from the redistribution of electrons within the fully overlapping potential spaces. It generates positive cations and negative anions, as are obtained by partitioning molecular densities (Maslen and Spackman 1985) which are commonly understood in accounting for such physical properties as ferroelectricity.

This understanding of the precursors to bonding provided by the promolecule model differs conceptually from those invoked in most descriptions of charge transfer. However, its general applicability, extending to bonds of all orders involving atoms for the whole periodic table, makes it a valuable starting point for developing a self-consistent picture of charge transfer. It gives a more convincing description of charge transfer processes than models constructed from free ion wavefunctions.

Acknowledgments

The assistance of Victor Streltsov is gratefully acknowledged. This work has been supported by the Australian Research Grants Scheme.

References

Balint-Kurti, G. G., and Karplus, M. (1974). *In* 'Orbital Theories of Molecules and Solids' (Ed. A. March) (Clarendon Press: Oxford).
Buttner, R. H., and Maslen, E. N. (1988). *Acta Crystallogr.* C **44**, 1707.
Clementi, E., and Roetti, C. (1974). *Atomic Data Nucl. Data Tables* **14**, 177.
Gordon, R. G., and Kim, Y. S. (1972). *J. Chem. Phys.* **56**, 3123.
Hall, S. R., King, G. S. D., and Stewart, J. M. (Eds) (1995). 'Xtal3·4 User's Manual' (University of Western Australia, Lamb, Perth and Maryland, USA).
Harrison, W. A. (1980). 'Electronic Structure and the Properties of Solids' (Freeman: San Francisco).
Hirshfeld, F. L. (1977*a*). *Theoret. Chim. Acta* **44**, 129.
Hirshfeld, F. L. (1977*b*). *Israel J. Chem.* **16**, 198.
Hirshfeld, F. L., and Rzotkiewicz, S. (1974). *Molec. Phys.* **27**, 1319.
Hohenberg, P., and Kohn, W. (1964). *Phys. Rev.* B **136**, 864.
Huber, K. P., and Herzberg, G. (1979). 'Molecular Spectra and Molecular Structure. IV. Constants of Diatomic Molecules' (Van Nostrand–Reinhold: New York).
Kittel, C. (1986). 'Introduction to Solid State Physics', 6th edn, Chapt. 3 (Wiley: New York).
Maksic, Z. B. (1984). *Croat. Chem. Acta* **57**, 1295.
Mann, J. B. (1988). Personal communication.
Mann, J. B., and Waber, J. T. (1973). *Atomic Data* **5**, 210.
Maslen, E. N., and Spackman, M. A. (1985). *Aust. J. Phys.* **38**, 273.
Moore, F. J. A. (1939). 'History of Chemistry', 3rd edn (McGraw–Hill: New York, London).
Partington, J. R. (1939). 'A Short History of Chemistry' (Macmillan: London).
Partington, J. R. (1964). 'A History of Chemistry', Vol. 4 (Macmillan: London).
Sargent-Welch Scientific Company (1980). 'Table of Periodic Properties of the Elements'. Catalog Number S-18806.
Sherman, J. (1932). *Chem. Reviews* **11**, 93.
Spackman, M. A., and Maslen, E. N. (1986). *J. Phys. Chem.* **90**, 2020.
Tosi, M. P. (1964). *Solid State Phys.* **16**, 1.
Trefry, M. G., Maslen, E. N., and Spackman, M. A. (1987). *J. Phys.* C **20**, 19.
Tsirelson, V. G., and Ozerov, R. P. (1996). 'Electron Density and Bonding in Crystals' (IOP Publishing: Bristol).
Wedepohl, P. T. (1967). *Proc. Phys. Soc. London* **92**, 79.
Zachariasen, W. H. (1931). *Z. Kristallogr.* **80**, 137.

Manuscript received 2 March, accepted 24 August 1999